A nonlinear beam model to describe the postbuckling of wide neo-Hookean beams

Luuk A. Lubbers, Martin van Hecke and Corentin Coulais

Huygens-Kamerlingh Onnes Lab, Universiteit Leiden, PObox 9504, 2300 RA Leiden, The Netherlands

FOM Institute AMOLF, Science Park 104, 1098 XG Amsterdam, The Netherlands

Abstract

Wide beams can exhibit subcritical buckling, i.e. the slope of the force-displacement curve can become negative in the postbuckling regime. In this paper, we capture this intriguing behaviour by constructing a 1D nonlinear beam model, where the central ingredient is the nonlinearity in the stress-strain relation of the beam's constitutive material. First, we present experimental and numerical evidence of a transition to subcritical buckling for wide neo-Hookean hyperelastic beams, when their width-to-length ratio exceeds a critical value of 12%. Second, we construct an effective 1D energy density by combining the Mindlin-Reissner kinematics with a nonlinearity in the stress-strain relation. Finally, we establish and solve the governing beam equations to analytically determine the slope of the force-displacement curve in the postbuckling regime. We find, without any adjustable parameters, excellent agreement between the 1D theory, experiments and simulations. Our work extends the understanding of the postbuckling of structures made of wide elastic beams and opens up avenues for the reverse-engineering of instabilities in soft and metamaterials.

Keywords: Postbuckling, Nonlinear elastic materials, Wide beam theory

1. Introduction

Recent years have seen an upsurge of interest in the instabilities and postinstability behaviour of flexible structures. Rather than seeing instabilities as failure, they recently have been leveraged to achieve novel functional (meta)materials and structures (Reis, 2015; Reis et al., 2015). As such, materials and structures featuring snapping (Holmes and Crosby, 2007; Florijn et al., 2014), wrinkling (Terwagne et al., 2014; Danas and Triantafyllidis, 2014), fingering (Biggins et al., 2013) or buckling (Mullin et al., 2007; Shim et al., 2012; Coulais et al., 2015) have been created. Collectively they constitute a promising route to develop mechanical devices for sensing (Brenner et al., 2003; Coulais et al., 2016), actuation (Wang et al., 2012; Li et al., 2013; Terwagne et al., 2014; Overvelde et al., 2015) or soft robotics (Autumn et al., 2000; Shepherd et al., 2011).

These structures harness postinstabilities *and* their constituents undergo large deformations. A theoretical description of this regime, where as we will show nonlinearities are key, is not well developed yet. On the one hand, the description of postbuckling behaviour has been widely investigated, but for models in which the constitutive material is assumed to be linearly elastic under small deformations (Hutchinson and Koiter, 1970; Budiansky, 1974; Davies et al., 1994; Magnusson et al., 2001; Vaz and Silva, 2003; Mazzilli, 2009; Bažant and Cedolin, 2010; Humer, 2013). On the other hand, much attention has been devoted to characterizing the instabilities of nonlinear elastic cellular materials (Geymonat et al., 1993; Lopez-Pamies and Castañeda, 2006b,a; Michel et al., 2007) or structures (Goriely et al., 2008), but only for the onset of instability, and not for the postinstability regime.

Euler buckling, known as the phenomenon where an elastic beam will buckle under a sufficiently large compressive axial load, is perhaps the simplest and the most widespread instability (Euler, 1774). Much theoretical attention has been devoted to describing it using the classical (Timoshenko and Gere, 1961; Reiss, 1969), extensible and shearable (Antman, 1972) elastica problem. Further in-depth studies have focused on the onset of buckling, the structure of buckled states (Antman and Rosenfeld, 1978; Antman and Pierce, 1990), closed form solutions (Goto et al., 1987, 1990; Pflüger, 2013), large deformations (Simo and Vu-Quoc, 1988; Wang, 1997; Irschik and Gerstmayr, 2009) and three-dimensional (Reissner, 1973; Simo, 1985; Simo and Vu-Quoc, 1986, 1991) deformations. In this paper we investigate the postbuckling regime of wide beams, where strains are necessarily large. A salient feature of buckling of slender beams is that the postbuckling compliance increases tremendously after buckling, yet remains positive. However, in recent work we showed that wide beams that buckle and undergo large deformations can exhibit a negative postbuckling compliance (Coulais et al., 2015). Although negative compliance is commonly observed in buckling of shells (Bažant and Cedolin, 2010), pipes (Hutchinson and Koiter, 1970) and the wrinkling of membrames (Pocivavsek et al., 2008; Diamant and Witten, 2011; Audoly, 2011), it has not been reported for beam buckling, and to the best of our knowledge is not predicted by existing beam models.

Here we develop a 1D nonlinear beam model, that without adjustable parameters, describes the postbuckling slope of wide neo-Hookean beams. In particular, this model allows to analytically capture the onset of subcritical buckling (postbuckling slope < 0) for widths larger than approximately 15%, in good agreement with experiments and FEM simulations. In Section 2 we expand on our previous experimental and numerical findings to show that for neo-Hookean beams, the postbuckling compliance becomes negative when the beam width-to-length ratio t exceeds approximately 12% (Coulais et al., 2015). In Section 3 we construct an effective 1D energy density by combining the Mindlin-Reissner kinematics (Reissner, 1972) with a nonlinearity in the stress-strain relation and establish the governing beam equations. We then solve the beam equations to obtain the variation of the postbuckling slope with t and find that, without any adjustable parameters, our model is in excellent agreement with experiments

and simulations. Our work thus unambigously unravels the link between stress-strain nonlinearity and postbuckling behaviour. While we focus on the buckling of wide neo-Hookean beams, we note that we only need to include quadratic corrections to the stress-strain relation to correctly capture the physics. Hence, for materials with other nonlinear constitutive laws, including metamaterials as explored in Coulais et al. (2015) and Coulais (2016), our description is also valid. Our analytical description can be used to rationally design the postbuckling behaviour of beams, and we hope that it can inspire work to capture and describe postinstability behaviours of other elastic systems. More widely, our work may impact the design of compliant devices, which harness instabilities (e.g. buckling, snapping, wrinkling) to convey mechanical functionalities that are of use in soft robotics (Autumn et al., 2000; Shepherd et al., 2011), sensors (Brenner et al., 2003; Coulais et al., 2016) and actuators (Wang et al., 2012; Li et al., 2013; Terwagne et al., 2014; Overvelde et al., 2015).

2. Phenomenology: Subcritical Buckling

In this section, we present and expand the findings from our previous work on subcritical buckling of wide beams (Coulais et al., 2015). First, we discuss both the experimental and numerical protocols to study buckling of rectangular beams to determine the force-displacement relation. We consider both the numerical protocol for 3D FEM simulations with boundary conditions that closely model the experimental conditions, and 2D simulations with simplified boundary conditions. Second, we analyze the onset of buckling and the postbuckling compliance of beams of varying width-to-length ratio t. We then show that for both experiments and numerics the postbuckling compliance varies systematically with t, and becomes negative for $t \gtrsim 0.12$.

2.1. Experiments and FEM simulations

In the analysis below, we consider beams of the width-to-length ratio $t = w/\ell$ and depth d, under load F and corresponding uniaxial displacement u, where $u, F > 0$ correspond to a compressive deformation (Fig. 1a and b).

2.1.1. Experiments

To perform buckling experiments, we mold 12 solid rectangular beams of rest length $\ell = 45$ mm, depth $d = 35$ mm and widths ranging from $w = 1.55$ mm to $w = 12.85$ mm (Fig. 1(a)) out of a well-characterized silicon rubber (Zhermarck, Polyvinyl Siloxane double elite 8, density 1.15×10^3 kg/m^3, Young's modulus $E = 250$ kPa, Poisson's ratio $\nu \approx 0.5$). The extremities of the beams are glued on plexiglass plates that are attached to the uniaxial testing device (Instron 5965) in order to approximate clamped-clamped boundary conditions, and we perform the experiments in a water bath in order to limit the effects of gravity.

2.1.2. 3D simulations

We simultaneously carry out a nonlinear analysis using the commercial finite element package ABAQUS/STANDARD on beams with the exact same geometry as in the experiments. We determine the buckling point using a specific algorithm in our finite element code that does not require seeding the initial geometry with imperfections (Coulais et al., 2015), allowing to obtain a 0.1% accuracy on the buckling onset.

Material model — The rubbers used in our experiments are well described by the incompressible neo-Hookean formulation of nonlinear elasticity (Boyce and Arruda, 2000). We therefore use a neo-Hookean strain energy density (Ogden, 1997) of the form

$$W = \frac{G}{2}\left(\det(\mathbf{F})^{-2/3}\mathrm{tr}(\mathbf{F}\mathbf{F}^{\mathbf{T}}) - 3\right) + \frac{K}{2}(\det(\mathbf{F}) - 1)^2, \tag{1}$$

where G is the shear modulus, K the bulk modulus and $\mathbf{F} \equiv \partial\mathbf{x}/\partial\mathbf{X}$ is the deformation gradient tensor from the undeformed coordinates $\mathbf{X}$ to the deformed coordinates $\mathbf{x}$. In the numerical analysis, we use the moduli $G = 83$ kPa and $K = 42$ GPa, which models accurately the $E = 250$ kPa nearly-incompressible rubber used in the experiments.

Boundary conditions — We numerically impose clamped-clamped boundary conditions to resemble the experiments where the endpoints of the beam are glued on plexiglass plates.

2.1.3. Simplified 2D FEM simulations

In addition, we carry out 2D plane stress simulations (Abaqus element type CPS4) using the same material model, yet with simplified slip boundary conditions at both endpoints of the beam, which allows for free lateral expansion at the clamped-clamped endpoints to avoid barreling effects (Narayanasamy et al., 1988). The choice for plane stress over plane strain conditions is a priory not obvious because our beams are intermediate between the plane stress limit ($w \gg d$), and plane strain limit ($w \ll d$). We therefore used our 3D simulations to investigate the 3D stresses and strains for beam thicknesses where the postbuckling slope changes sign ($t \approx 0.1$). We found that in this case there are significant out of plane strains, but that the out of plane stresses are small (ratio between the lateral and uniaxial stresses < 0.1) – this motivates us to focus on the plane stress case. The plane stress condition, which is nontrivial in finite-strain elasticity, is implemented by requiring that the yy-component of the true (Cauchy) stress is zero, which necessitates the iterative computation of the deformation gradient component F_{yy} to satisfy this condition (Doghri, 2013). Altogether, these assumptions ensure that more complex 3D and boundary effects can be neglected and allow us to carry out the analysis in the simplest setting where subcritical buckling can be observed, and will be used later to

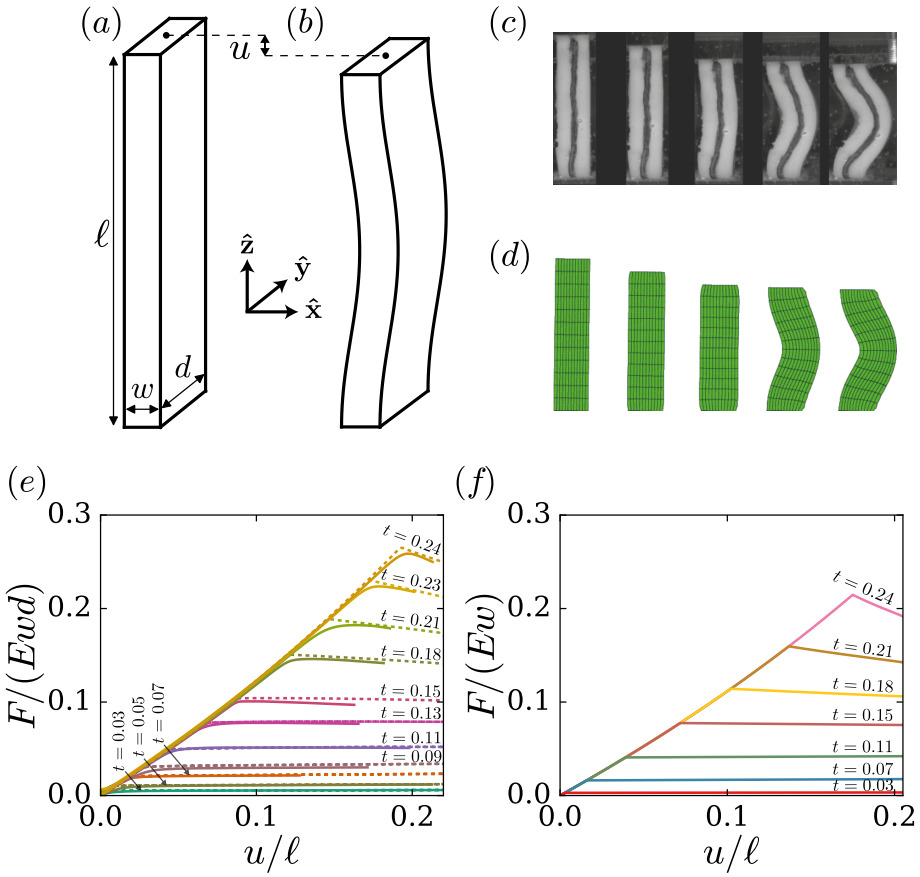

Figure 1: Buckling of wide neo-Hookean beams. (a) Sketch of a beam in its initial undeformed state, for which the beam has a rest length ℓ, width w and depth d. (b) Applying a compressive displacement u, leads to compression and eventually buckling of the beam. (c-d). Frontview snapshots of (c) the experiment and (d) the simulation for a beam of length $\ell = 45$ mm, depth $d = 35$ mm and width $w = 11.95$ mm, at compressive displacements (from left to right) $u = 0$, $u = 0.5\ u_c$, $u = 0.99\ u_c$, $u = 1.1\ u_c$ and $u = 1.2\ u_c$. (e-f) Scaled compressive force $F/(Ewd)$ vs. compressive displacement u/ℓ for beams of different width for (e) the experiments (solid lines) and 3D simulations (dashed lines) and (f) the simplified 2D simulations. As the effects of gravity are negligible in the experiments and absent in simulations, the choice of the Young's modulus E is immaterial and we trivially scale the forces by E.

pinpoint the physical mechanism at stake in the postbuckling behaviour of wide beams.

2.2. Buckling and Subcritical Buckling

In Fig. 1(c-d) we simultaneously display 5 frontview snapshots of experiments and 3D simulations for a beam with $t = 0.23$ ($w = 10.20$ mm) at different compressive displacements, which are in very good qualitative agreement. Moreover,

we plot the obtained force-displacement curves for the complete range of beam widths in Fig. 1(e), which illustrates that 3D simulations and experiments are also in very good quantitative agreement. Hence, the neo-Hookean material model describes the buckling of wide beams well. For all curves, we observe a near-linear increase until the onset of buckling, at which the slope abruptly changes. For thin beams, the force increases after buckling, while for thick beams, the force decreases. For buckling experiments under controlled force of a sufficiently wide beam, the postbuckling branch would thus be unstable and the pitchfork instability would be subcritical. Therefore, we refer to this type of instability as *Subcritical Buckling*. The 2D simulations, albeit considerably simpler, display qualitatively similar behaviour (Fig. 1(f)), which demonstrates that subcritical buckling does originate neither from boundary-induced singularities nor from 3D effects. To the best of our knowledge, although subcritical buckling is fairly common in other settings such as the wrinkling instability (Moon et al., 2007; Huang et al., 2007; Cao and Hutchinson, 2011) and the wrinkle-to-fold transition (Pocivavsek et al., 2008; Diamant and Witten, 2011; Audoly, 2011), such sign change is not predicted by any theory as of now for the Euler buckling of wide beams for realistic aspect ratios. Note that Magnusson et al. (2001) predicted such transition from supercritical to subcritical postbuckling, yet for overly large aspect ratios (t=0.24), and for which the validity of the extensible, non-shearable elastica is not guaranteed.

We now retrieve the onset of buckling u_c and the postbuckling slope S, using the relation between the load F and the compressive displacement u in the postbuckling regime:

$$\frac{F - F_c}{F_c} = S\frac{(u - u_c)}{\ell} + \mathcal{O}\left((u - u_c)^2\right), \tag{2}$$

with F_c the critical buckling force. In Fig. 2(a) we display the onset of buckling as a function of the beam width-to-length ratio t, for the experiments, 3D FEM simulations and the 2D FEM simulations, and observe quantitative agreement with the prediction of Euler's elastica for clamped-clamped boundary conditions, $u_c^{euler}/\ell = t^2\pi^2/3$ (Bažant and Cedolin, 2010). While the onset shows quantitative agreement with Euler's prediction, the results in Fig. 2(b) show the postbuckling slope S strongly deviates from Euler's prediction $S = 1/2$ as t increases, and becomes *negative* for $t \gtrsim 0.12$. Importantly, Fig. 2(b) illustrates that subcritical buckling of wide beams is a robust phenomena: Even with the simplifications made in the 2D simulations, the differences in the postbuckling slope between 2D and 3D simulations are modest.

The emergence of subcritical Euler buckling is, as we will show, readily related to nonlinearity in the stress-strain relation (Coulais et al., 2015). In the following, we will rationalize such behaviour by constructing a 1D model that encompasses such a stress-strain nonlinearity.

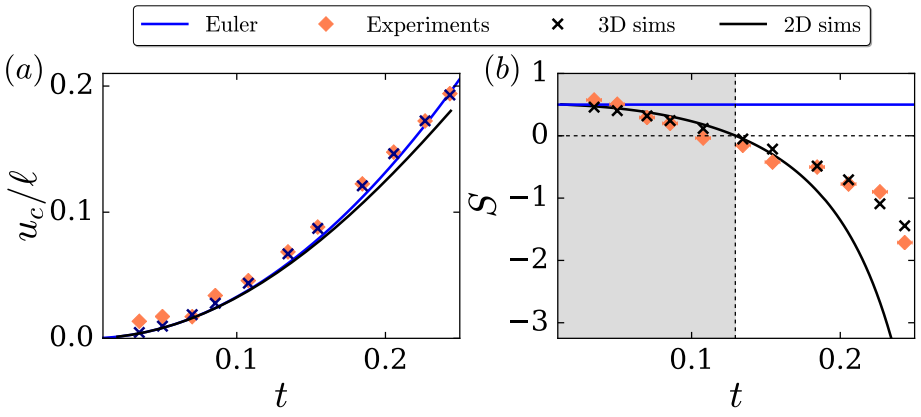

Figure 2: Critical compressive displacement and postbuckling slope as function of the beam width-to-length ratio, for Euler's elastica (solid blue), experiments (orange diamonds), 3D FEM simulations (black crosses) and 2D plane stress FEM simulations (solid black). (a) The onset of buckling, u_c, in experiments and simulations qualitatively follows Euler's elastica. (b). The postbuckling slope S in experiments and simulations progressively deviates from the Euler limit $S = 1/2$ for large t. Subcritical buckling ($S < 0$) occurs for $t \gtrsim 0.12$, indicated by the shaded region.

3. 1D nonlinear beam model

In this section we formulate a 1D nonlinear model to describe the postbuckling of wide beams. Our model assumes (i) that the kinematics of the 1D model are captured by the Mindlin-Reissner strains, namely axial strain, curvature and shear (Reissner, 1972); (ii) that axial stress and strain are related nonlinearly. Based on these assumptions, we derive an expression for the 1D energy density as well as the governing equations for the mechanical equilibrium of wide beams. We then analytically solve the governing equations and find excellent agreement with 2D simulations for the postbuckling behaviour, without any adjustable parameters. Finally, we refine our beam model using extensive 2D simulations and show that distortions from Mindlin-Reissner kinematics have a negligible effect on the predictions by the model.

3.1. Mindlin-Reissner beam with a nonlinear stress-strain relation

Mindlin-Reissner kinematics describe beams that can be compressed, bent and sheared. These three deformation modes are quantified by a compressive $\tilde{\varepsilon}_0(s)$, curvature $\varepsilon_1(s) \equiv \theta_s(s)$ and shear strain $\gamma_0(s)$, as function of the curvilinear coordinate s along the beam's central axis, with θ the deflection angle of the beam's axis with respect to the vertical. Therefore the total elastic energy of

these beams is a functional of the form

$$\mathcal{E}\left[\tilde{\varepsilon}_0(s), \theta(s), \varepsilon_1(s), \gamma_0(s)\right] = \int_0^\ell ds\, \epsilon\left[s, \tilde{\varepsilon}_0(s), \theta(s), \varepsilon_1(s), \gamma_0(s)\right], \tag{3}$$

where the 1D energy density of the beam $\epsilon\left[s, \tilde{\varepsilon_0}(s), \theta(s), \varepsilon_1(s), \gamma_0(s)\right]$ exclusively depends on these strains.

The second key assumption is that stress and strain are related nonlinearly. To describe the vicinity of postbuckling, we set up an expansion of the nominal stress σ around the buckling strain ε_b up to quadratic order, which yields:

$$\frac{\sigma - \sigma_b}{E_b} = (\varepsilon - \varepsilon_b) + \eta\,(\varepsilon - \varepsilon_b)^2 + \mathcal{O}\,(\varepsilon - \varepsilon_b)^3, \tag{4}$$

where E_b and σ_b are the effective Young's modulus and nominal stress at buckling. In the case of neo-Hookean materials under plane stress conditions, the coefficients of this expansion can be determined analytically and read $\eta = -1 + \mathcal{O}\,(\varepsilon_b)$ and $E_b = E + \mathcal{O}\,(\varepsilon_b)$ (See Appendix A.3 for a demonstration). In the case of plane strain conditions, not considered here, it can be shown that $\eta = -3/2 + \mathcal{O}\,(\varepsilon_b)$ (See SI in Coulais et al. (2015)). The nonlinearity of the above stress-strain relation stems from the combination of large deformations and incompressibility and can qualitatively be understood from the fact that upon compression (tension) the cross-sectional area increases (decreases) and the stress-strain curve is therefore effectively stiffening (softening). In addition, we assume a linear relation between the nominal shear stress τ and shear strain γ, $\tau = G\gamma$ in agreement with the elasticity of neo-Hookean materials (Ogden, 1997).

Based on these two assumptions, we find that the 1D energy density describing postbuckling reads:

$$\begin{aligned}\epsilon\left[\varepsilon_0(s), \varepsilon_1(s), \gamma_0(s)\right] =& E_b A\, \varepsilon_b\, \varepsilon_0 + \frac{1}{2} E_b A \varepsilon_0^2 \\ &+ E_b I \left(\frac{1}{2} + \eta\, \varepsilon_0\right) \varepsilon_1^2 \\ &+ \frac{GA}{2}\, \gamma_0^2,\end{aligned} \tag{5}$$

with $\varepsilon_0(s) = \tilde{\varepsilon}_0(s) - \varepsilon_b$, $A = wd$ (the cross-sectional area) and G is the shear modulus. Crucially, the nonlinear correction proportional to η introduces a nonlinear coupling between the compression strain and the curvature $\varepsilon_0 \varepsilon_1^2$, and such coupling is absent in previous linear beam models (Magnusson et al., 2001; Humer, 2013).

To establish the governing beam equations, the total elastic energy $\mathcal{E}$ has to be minimized under the geometrical constraint set by the boundary conditions. In the case of Euler buckling, a uniaxial displacement is applied along the vertical axis of the beam and is associated to the following geometrical constraint:

$$\Pi = F\left(u - \left(\ell - \int_0^\ell ds\, \left((1 + \varepsilon_b + \varepsilon_0)\cos\theta - \gamma_0 \sin\theta\right)\right)\right), \tag{6}$$

where F is the Lagrange parameter associated with the axial displacement u that corresponds to the external axial force applied on the beam. We use the fact that $\varepsilon_1 \equiv \theta_s$ to apply the Euler-Lagrange formulation (Marion, 2013) on the energy functional including the constraint:

$$\tilde{\mathcal{E}}\left[\varepsilon_0(s), \theta(s), \varepsilon_1(s), \gamma_0(s)\right] = \int_0^\ell ds\ \epsilon - \Pi, \tag{7}$$

which yields the governing equations of the beam:

$$E_b I \theta_{ss} + F\left\{(1+\varepsilon_b+\varepsilon_0)\sin\theta + \gamma_0\cos\theta\right\} + 2\eta E_b I\left(\theta_s \varepsilon_0\right)_s = 0, \tag{8a}$$

$$F\cos\theta + E_b A\left(\varepsilon_b+\varepsilon_0\right) + \eta E_b I \theta_s^2 = 0, \tag{8b}$$

$$GA\gamma_0 - F\sin\theta = 0. \tag{8c}$$

This set of three coupled equations determine the beam's central axis in the postbuckling regime of wide beams. We will refer to this set of equations as the 1D *nonlinear* beam model, since it includes the nonlinearity η.

Please note that in the limit of linear materials ($\eta = 0, E_b = E$), Eqs. (8) correspond to the equations for a shearable and extensible beam derived by (Humer, 2013). If additionally the beam is assumed non-shearable, $\gamma_0(s) = 0$ and Eq. (8c) drops out, leaving us with a simpler model derived by (Magnusson et al., 2001). Finally, for inextensible beams $\varepsilon_0(s) = \varepsilon_b = 0$, Eq. (8b) drops out, and we recover Euler's elastica $EI\theta_{ss} + F\sin\theta = 0$ (Euler, 1774). Our beam model thus correctly captures all these linear models.

3.2. Solutions to the 1D nonlinear beam model

In this section we solve the 1D nonlinear beam model given in Eqs. (8) and show that the postbuckling slope is dramatically changed and the compressive Mindlin-Reissner strain significantly improved, when incorporating a nonlinearity η.

3.2.1. Dimensionless form

The results below will be presented in dimensionless form and we introduce the following dimensionless quantities:

$$\bar{s} = \frac{s}{\ell}; \qquad \bar{F} = \frac{F\ell^2}{E_b I}; \qquad \Lambda^{-2} = \frac{I}{A\ell^2}. \tag{9}$$

The quantities $\bar{s}$ and $\bar{F}$ represent the dimensionless curvilinear coordinate and force respectively, and $\Lambda \sim \ell/w$ can be recognized as the slenderness ratio (Bažant and Cedolin, 2010). Using the dimensionless quantities, the set of scaled beam equations given in Eqs. (8) reads:

$$\theta_{\bar{s}\bar{s}} + \bar{F}\left\{(1+\varepsilon_b+\varepsilon_0)\sin\theta + \gamma_0\cos\theta\right\} + 2\eta(\theta_{\bar{s}}\ \varepsilon_0)_{\bar{s}} = 0, \tag{10a}$$

$$\varepsilon_0 = -\left(\bar{F}\Lambda^{-2}\cos\theta + \eta\Lambda^{-2}\theta_{\bar{s}}^2 - \varepsilon_b\right), \tag{10b}$$

$$\gamma_0 = \bar{F}\Lambda^{-2}\frac{E_b}{G}\sin(\theta). \tag{10c}$$

In the remainder of the paper we drop the overbars, unless if noted otherwise. For convenience, we additionally define:

$$r \equiv \frac{E_b}{G} = 2\left(1+\nu\right) + \mathcal{O}\left(\varepsilon_b(t)\right), \tag{11}$$

where ν is the Poisson ratio.

In Eqs. (10) we use Euler's prediction for ε_b, that accurately describes the onset of buckling, even for wide beams (see Fig. 2(a)). Furthermore, all the parameters E_b, r and η can be determined theoretically to leading order in the beam width-to-length ratio t. In what follows we use these predictions as input parameters and solve Eqs. (10) to obtain a closed-form expression for the postbuckling slope as function of and to leading order in t.

3.2.2. Closed-form expression for the postbuckling slope as a function of t.

Here we derive our main result, namely the postbuckling slope as a function of beam width-to-length ratio t. In deriving the postbuckling slope, we are interested only in the mechanical response of the beam infinitesimally beyond buckling. Therefore, we only need to solve Eq. 10 for small ($\theta(s) \ll 1$), yet nonlinear beam deflections. As a first step, we expand the governing beam equations up to the cubic order in θ, and substitute Eqs. (8b-8c) into Eq. (8a) to obtain:

$$\begin{aligned} 0 = \theta_{ss}&\left(1 - 2\eta\left(F\Lambda^{-2} + \varepsilon_b\right) - 6\theta_s^2\Lambda^{-2}\eta^2\right) + \theta\left(F + \left(r-1\right)F^2\Lambda^{-2}\right) \\ &- \theta^3\left(\frac{1}{6}F + \frac{2}{3}\left(r-1\right)F^2\Lambda^{-2}\right) + \theta^5\left(\frac{1}{12}F^2\Lambda^{-2}\left(r-1\right)\right) \\ &+ \left(\theta^2\theta_{ss} + \theta\theta_s^2 + \frac{1}{6}\theta^3\theta_s^2\right)F\Lambda^{-2}\eta. \end{aligned} \tag{12}$$

We now solve this linearized equation using a perturbative expansion that is consistent with the symmetry of Eq. (12), which only contains odd powers in θ, and that matches the imposed clamped-clamped boundary conditions, $\theta(0) = \theta(1) = 0$:

$$\theta(s) = \alpha \sin 2\pi s + \beta \sin 6\pi s. \tag{13}$$

Here, α and β physically correspond to the maximum deflection angle of the first and third harmonic of the Fourier series which describe the beam shape $\theta(s)$. To see how α and β are coupled, we substitute the perturbative expansion for $\theta(s)$ in Eq. (12). By collecting all terms proportional to $\sin(6\pi s)$, and setting the sum of their coefficients to zero, we found that β is coupled to a higher power of α, specifically $\beta \sim \alpha^3$. Therefore, since $\alpha \ll 1$, $\beta \ll \alpha$, and in the following we set $\beta = 0$.

Under the assumption $\beta = 0$, Eq. (12) leads to an explicit equation relating the force F to the deflection α. Expanding $F(\alpha)$ for small deflection α, yields the shape of the pitchfork bifurcation (Guckenheimer and Holmes, 1983):

$$F(\alpha, \Lambda, \eta, r) = F_c + \kappa\alpha^2 + \mathcal{O}(\alpha^4), \tag{14}$$

where κ is the curvature of the pitchfork. To connect this excess force to the axial displacement u, we establish the relation between the deflection angle α and the axial displacement using the geometrical relation

$$u/\ell = 1 - \int_0^1 ds\,\{(1 + \varepsilon_b + \varepsilon_0)\cos\theta - \gamma_0 \sin\theta\}, \tag{15}$$

which upon small deflections, can be expanded to obtain the desired relation $u(\alpha, F, \Lambda, \eta, r)$. We then invert this relation to $\alpha(u, F, \Lambda, \eta, r)$ and substitute it in Eq. (14), resulting in an equation that needs to be solved for $F(u, \Lambda, \eta, r)$. The final step is then to expand the solution for F in the limit $u \to u_c^+$, which leads to an equation of the form as in Eq. (2), with the postbuckling slope S equal to:

$$S = \frac{1}{2} - \left(\frac{1}{12} + 2\eta^2\right)\pi^2\, t^2 + \mathcal{O}(t^4). \tag{16}$$

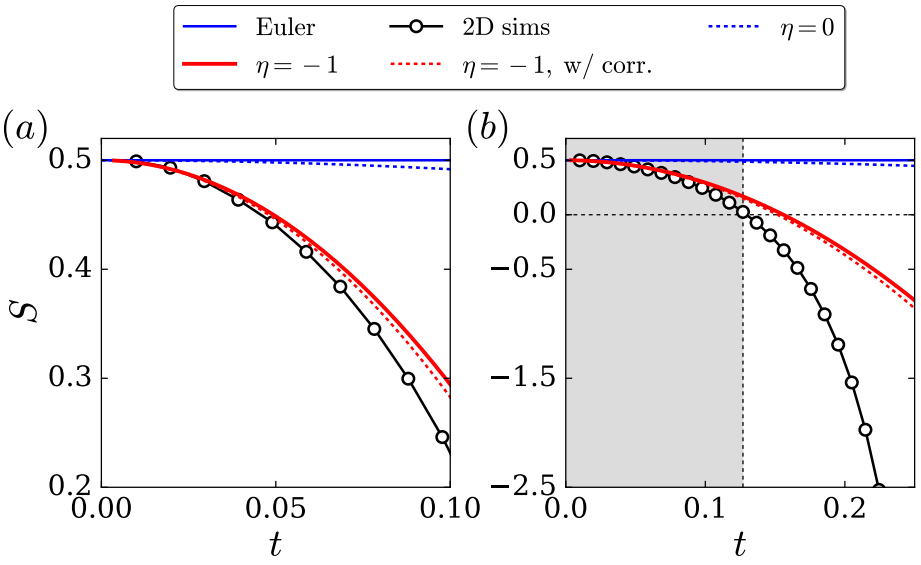

Figure 3: Postbuckling slope S as function of the beam width-to-length ratio t, for five different models. In the Euler limit $S = 1/2$, while in 2D simulations (open circles) S varies with t. Solutions to our model given in Eq. (16) are shown for $\eta = 0$ (dashed blue) and $\eta = -1$ (solid red). Finally, we also show data for an extension of our model discussed in Section 3.3 (dashed red). (a-b) Panel (a) shows a closeup for $0 < t < 0.10$ and panel (b) shows a wider range of width-to-length ratio ($0 < t < 0.25$). The shaded region indicates the cross-over to subcritical buckling ($S < 0$) for the 2D simulations.

This result confirms that Euler's elastica prediction ($S = 1/2$) is recovered in the limit of slender beams ($t \to 0$) and shows that the leading order correction to the postbuckling slope S is quadratic in t. Notice that such correction comprises the stress-strain nonlinearity η. Does this correction bring an improvement for the prediction of the postbuckling slope? To check this, we compare the value of the postbuckling slope S obtained from 2D simulations to the prediction of Eq. (16), where the value of η is independently determined using the neo-Hookean model under the simplifying assumption that the neo-Hookan material is uniaxially compressed (see Appendix A.3). The comparison shown in Fig. 3 shows excellent agreement between the simulations and our prediction in Eq. (16), namely the quadratic correction matches the data very well for small t and remains accurate up to $t \approx 0.1$ (see Fig. 3(a)). Although we should not expect our prediction to be accurate for wider beams, it remains in qualitatively agreement with the simulations and succeeds in predicting subcritical buckling at a critical width-to-length ratio $t \approx 0.15$ (see Fig. 3(b)).

Beyond the success of our asymptotic approach, a closer inspection of the quadratic correction to the postbuckling slope S in Eq. (16) allows us to infer three important conclusions. First, the quadratic correction is independent of the ratio of moduli r, given in Eq. (11). Since r sets the magnitude of shear deformations with respect to uniaxial compression, we conclude that shear is subdominant in the lowest order terms of $S(t)$. Second, the coefficient of the quadratic correction is quadratic in η (see Fig. 5), suggesting the sign of the nonlinearity does not play a role. This is consistent with earlier simulations and experiments (Coulais et al., 2015) where we designed metabeams for which $\eta > 0$, in contrast to the neo-Hookean stress-strain nonlinearity for which $\eta < 0$, and found that also in this case S decreases with t. Third, the coefficient of the quadratic correction confirms our initial hypothesis that the stress-strain nonlinearity is the crucial ingredient to capture $S(t)$ correctly: the magnitude of this coefficient is entirely determined by the nonlinearity parameter η. In the absence of η the magnitude of the coefficient is much smaller, and $S(t)$ would be only weakly decreasing with t (see Fig. 3). We thus conclude that the nonlinearity η ensures that our theoretical prediction in Eq. (16) is able to capture the subcritical buckling at realistic aspect ratios, in contrast to earlier linear theories (Reissner, 1972; Magnusson et al., 2001; Humer, 2013).

3.2.3. Mindlin-Reissner strains in the nonlinear beam model

We will now illustrate that the prediction for the compressive Mindlin-Reissner strain $\varepsilon_0(s)$ is significantly improved by the nonlinearity η. In Fig. 4(a-c) we plot the compressive, bending and shear Mindlin-Reissner strain for the 2D simulations and the beam model in Eq. (8). First, panel (a) shows a significant qualitative difference in the Mindlin-Reissner strain $\varepsilon_0(s)$ between the linear and nonlinear beam model. In contrast to the linear beam model, the nonlinear beam model is in good qualitative agreement with the FEM simulations and the prefactors of the sinusoidal modulations all carry the same sign, albeit with a slightly smaller amplitude. This confirms our earlier assertion that the nonlin-

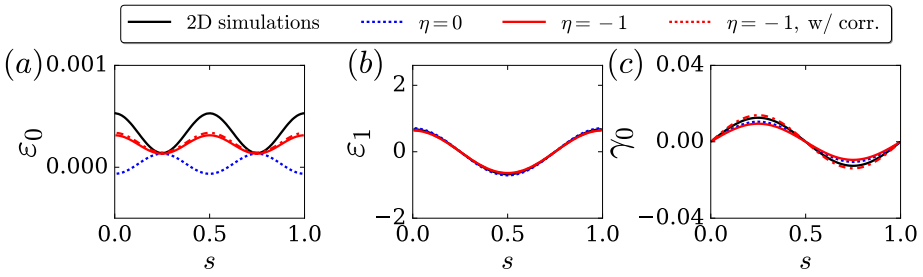

Figure 4: Mindlin-Reissner strains as a function of s, for 4 different models. We consider a wide ($t = 0.1$) beam which is compressed to an axial displacement of $u/u_c = 1.06$. We show results for 2D simulations (solid black), and compare them to numerical solutions to our beam model in Eqs. (8) for $\eta = 0$ (dashed blue) and $\eta = -1$ (solid red). Finally, we also show numerical solutions to an extension of our beam model in Eqs. (20) discussed in Section 3.3 (dashed red). (a-c) We have respectively plotted the compressive, bending and shear Mindlin-Reissner strain along the beam.

earity η is the crucial factor to capture correctly the large deformations of wide neo-Hookean beams. Finally, panel (b) and (c) show that the Mindlin-Reissner strains $\varepsilon_1(s)$ and $\gamma_0(s)$ remain essentially unchanged due to the nonlinearity and the model shows excellent agreement with the 2D simulations.

3.3. Distortions from Mindlin-Reissner kinematics with nonlinear stress-strain relation

The previous derivation of the 1D nonlinear beam model in Eqs. (8) is simple and directly follows from the use of two basic assumptions. In particular, using Mindlin-Reissner kinematics is a customary yet not controlled assumption. In this section, we investigate the validity of such a choice by using extensive numerical simulations and demonstrate that distortions from the Mindlin-Reissner kinematics systematically occur, modifying the 1D energy density and governing equations, albeit with a subdominant effect.

To explore deviations from Mindlin-Reissner strains, we investigate systematically the stress and strain profiles in Appendix A. In particular, we find that the axial strain profile at the center of the beam takes the form:

$$\varepsilon(x) - \varepsilon_b = \tilde{\varepsilon}_0 + \varepsilon_1 x + \varepsilon_2 x^2 + \varepsilon_3 x^3 + \cdots , \tag{17}$$

where $x \in [-\frac{w}{2}, \frac{w}{2}]$ is the transverse coordinate across the beam width. $\tilde{\varepsilon}_0$ and ε_1 are Mindlin-Reissner strains introduced in Section 3.1 and ε_i (with $i \geq 2$) correspond to distortions from a linear axial strain profile. In Appendix A we have also performed a similar systematic analysis for the shear profile.

Following the extensive simulations and thorough asymptotic analysis pro-

cedure in Appendix A, we find that the 1D energy density takes the form:

$$\begin{aligned}\epsilon\left[\varepsilon_0(s),\varepsilon_1(s),\gamma_0(s)\right] =& E_bA\,\varepsilon_b\,\varepsilon_0+\frac{1}{2}E_bA\left(1+\zeta_2(\eta)\right)\varepsilon_0^2\\ &+E_bI\left(\frac{1}{2}\left(1+\zeta_1(t)\right)+\eta\,\varepsilon_0\right)\varepsilon_1^2\\ &+\frac{GA}{2}\,\gamma_0^2\left(k_1+k_2\gamma_0^2\right),\end{aligned}\tag{18}$$

where the coefficients E_b, η, $\zeta_1(t)$, $\zeta_2(\eta)$, G, k_1 and k_2 can be determined numerically. Note that in the limit when ζ_1, ζ_2 and k_2 are zero, we recover Eq. (5). Eq. (18) is very similar to Eq. (5) and the numerical values of the coefficients E_b, η, and G match the values that come from the neo-Hookean material model (Ogden, 1997) (see Appendix A). In addition we see that the differences associated to distortions from the Mindlin-Reissner kinematics can be captured by the coefficients $\zeta_1(t)$, $\zeta_2(\eta)$, k_1 and k_2. While $k_1 = 0.67 \pm 0.15$ is a classical coefficient known as the shear correction factor (Timoshenko, 1921; Timoshenko and Goodier, 1970) whose value quantitatively matches Timosenko's prediction (Cowper, 1966; Hutchinson, 2000), $\zeta_1(t)$, $\zeta_2(\eta)$, and k_2 are undocumented and correspond to higher order distortions of the strain profiles. They have been determined in Appendix A as:

$$\zeta_1\left(t\right) = 6\left(t^2+t^4\right),\tag{19a}$$

$$\zeta_2\left(\eta\right) = -0.2-0.15\eta,\tag{19b}$$

$$k_2\left(t\right) = 0.0013t^{-4}.\tag{19c}$$

Note that even though $k_2(t)$ is singular for $t \to 0$, γ_0 scales as t^4, such that the product $k_2\gamma_0^4$ that arises in Eq. (18) is regularized for $t \to 0$. Nonetheless, we see that the distortions in Eqs. (19) introduce minor modifications of the prefactors in Eq. (18) and in what follows we show that they do not play a major role in the model.

We now carry out the same Euler-Lagrange approach as previously and find the refined governing equations:

$$\zeta_1(t)E_bI\theta_{ss}+F\left\{\left(1+\varepsilon_b+\varepsilon_0\right)\sin\theta+\gamma_0\cos\theta\right\}+2\eta E_bI\left(\theta_s\varepsilon_0\right)_s=0,\tag{20a}$$

$$F\cos\theta+E_bA\left(\varepsilon_b+\zeta_2(\eta)\varepsilon_0\right)+\eta E_bI\theta_s^2=0,\tag{20b}$$

$$GA\gamma_0\left(k_1+2k_2\gamma_0^2\right)-F\sin\theta=0.\tag{20c}$$

This set of equations is the equivalent of the previously established Eqs. (8a-8c) and has been determined through a well defined and rigorous set of assumptions. Unfortunately, the coefficients $\zeta_1(t)$, $\zeta_2(\eta)$ and k_2 have to be determined numerically. Following the procedure in Section we linearize and solve Eqs. (20) and find that

$$S=\frac{1}{2}+\frac{\left(-3+2\left(1+\zeta_2(\eta)\right)-24\eta^2\right)\pi^2}{12\left(1+\zeta_2(\eta)\right)}t^2+\mathcal{O}(t^4),\tag{21}$$

which reduces to Eq. (16) by setting $\zeta_2 = 1$. We have plotted Eq. (21) in Fig. 3 and see that the corrections ζ_1, ζ_2 and k_2 result in a minor improvement to the postbuckling prediction. Finally, we numerically solved Eqs. 20 to obtain the Mindlin-Reissner strains and plotted the result for $\eta = -1$ in Fig. 4. Again, we find that the corrections result in a minor improvement to the postbuckling prediction. Altogether, this illustrates that the corrections ζ_1, ζ_2 and k_2 have a subdominant contribution to the postbuckling behaviour.

4. Conclusions and discussion

We have presented a thorough investigation of the postbuckling of nonlinear elastic beams, using experiments, finite element simulations and theory. In particular we have focussed on subcritical buckling, where, for neo-Hookean beams, the slope of the force-displacement curve becomes negative beyond buckling when the beam width-to-length ratio exceeds 12%. The main result of this paper is a 1D nonlinear beam model that includes a material nonlinearity η. We constructed the model by building the beam's energy density using Mindlin-Reissner kinematics with a nonlinearity in the stress-strain relation, and demonstrated that this nonlinearity is crucial to accurately capture the postbuckling behaviour of wide beams and in particular to predict subcritical buckling. In contrast with previous works that have reported a significant effect of the ratio E/G on the flexure response (Goto et al., 1990) and the critical buckling force (Humer, 2013) of extensible and shearable beams, we found that E/G has a subdominant effect on the postbuckling slope.

Though our model has been established in the case of neo-Hookean mate-

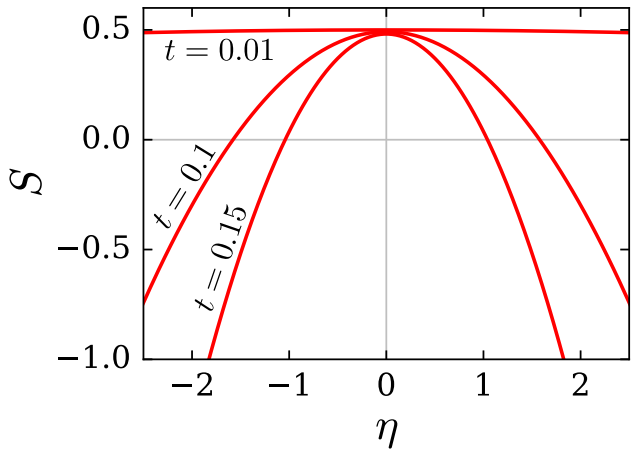

Figure 5: Postbuckling slope as a function of the nonlinearity η. Using Eq. (16) we have plotted $S(\eta)$ for $t = 0.01$, $t = 0.1$ and $t = 0.15$. The curves show that the postbuckling slope is quadratic in η and that the postbuckling slope does not exceed $S = 1/2$.

rial nonlinearity ($\eta < 0$), our findings could be generalized to a wider class of nonlinear elastic materials, such as cellular materials with nonlinear effective properties (Gibson and Ashby, 1997; Castañeda, 1991; Coulais, 2016). We expect this generalization to hold provided that the leading nonlinearity of the elastic material is quadratic in nature and that the material strains do not significantly deviate from the Mindlin-Reissner strain decomposition (as is shown in Section 3.3 for 2D plane stress beams). For example, in recent work by Coulais et al. (2015), beams patterned with a periodic 2D pattern of pores were shown to exhibit positive, geometrically induced nonlinearity ($\eta > 0$). They found that a sufficiently strong nonlinearity leads to subcritical buckling, even when the beam width-to-length ratio is small. Such a transition to subcritical buckling for $\eta > 0$ is in qualitative agreement with our theory that predicts that the postbuckling slope essentially decreases quadratically in η with its maximum at $\eta = 0$ (see Fig. 5). The present work rationalizes those findings and provide strong guidelines for the design of postinstability regimes in soft structures and architected materials (Ashby and Brechet, 2003), where arbitrary values of η can be achieved (Coulais, 2016). We envision in particular that our description could be of interest for the design of compliant hierarchical cellular materials, which often rely on the buckling instability for their functionality (Cho et al., 2014; Yang et al., 2016).

In addition, we note that other types of material nonlinearities could be explored and addressed within our framework, for instance, plasticity, stress-relaxation, swelling Yoon et al. (2010); Holmes et al. (2011); Kim et al. (2012); Pezzulla et al. (2015); Na et al. (2016) or even growth and activity, which are ubiquitous in biological solids (Gladman et al., 2016; Sharma et al., 2016)

Finally, while our work could be of great use for the engineering of systems that draw on Euler buckling for their functionality (Wang et al., 2014; Shim et al., 2012), a plethora of compliant architected material harness the *snapping* instability (Brenner et al., 2003; Holmes and Crosby, 2007; Shim et al., 2012; Nasto et al., 2013; Florijn et al., 2014; Overvelde et al., 2015; Frenzel et al., 2016; Raney et al., 2016; Coulais et al., 2017). In order to understand the role of materials nonlinearity on such instability and devise mechanical design guidelines, our present framework should be generalized to pre-curved geometries, such as curved beams and shells.

Acknowledgements

We acknowledge useful discussions with J.T.B. Overvelde and K.Bertoldi at the early stage of this work. It is a pleasure to thank J.T.B. Overvelde for the critical reading of our manuscript. We are grateful to the support by the Netherlands Organization for Scientific Research through a VICI grant (NWO-680-47-609).

Appendix A. Asymptotic Analysis of 2D FEM simulations

In this appendix, we use 2D FEM simulations to illustrate and quantify the role of nonlinearities in the stress-strain relation, set up a systematic series expansion for the spatial variation of stress and strain across the beam, and use the numerical results to determine the dominant terms in this expansion. Our findings will allow us to unambiguously establish a well defined expression for the 1D energy density of the beam and to compare it with standard limits such as Euler's elastic, Timoshenko beams and Mindlin-Reissner beams.

Appendix A.1. Series expansion of the axial nominal stress and strain

First, we perform a systematic expansion of the nominal stress and strain profiles in the beam's transverse coordinate x/w, the beam width-to-length ratio t and the excess displacement $\Delta u \equiv (u - u_c)/u_c$, and determine all prefactors and scaling exponents using our FEM results.

Standard beam theories such as Mindlin-Reissner theory assume that the nominal stress and strain profiles are linear in x. In wide 2D neo-Hookean beams, the deformation field is more complex and we analyze deviations from a linear profile by expanding the nominal strain and stress around the buckling strain (ε_b) and stress (σ_b), as function of the (scaled) transverse coordinate x/w, at the middle of the beam:

$$\varepsilon\left(t, \Delta u, \frac{x}{w}\right) - \varepsilon_b = \sum_{n=0} C_n\left(t, \Delta u\right)\left(\frac{x}{w}\right)^n, \tag{A.1a}$$

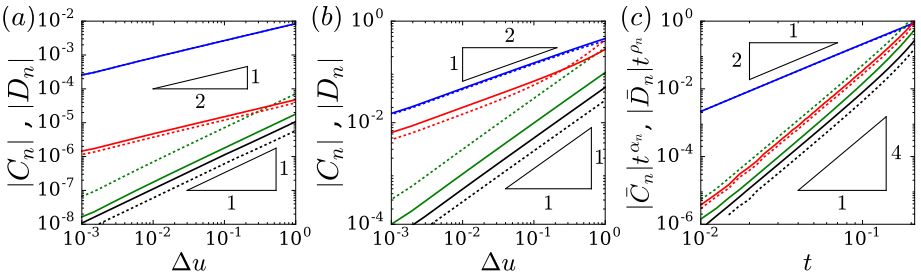

Figure A.6: Expansion of the nominal strain and stress profiles obtained by FEM simulations, according to Eqs. (A.2a-A.2b). We plot the postbuckling profile coefficients C_n and D_n in each order as a function of Δu and t. In black, blue, green and red we have plotted C_n (solid lines) and D_n (dashed lines), corresponding to the order $n = 0$, $n = 1$, $n = 2$ and $n = 3$ respectively. (a-b). We have plotted $|C_n|$ and $|D_n|$ as function of Δu for (a) a slender beam ($t = 0.02$) and (b) a thick beam ($t = 0.15$). (c). Dependence of C_n and D_n on the beam aspect ratio t.

	Δu		t	
n	β_n	τ_n	α_n	ρ_n
0	1.03 ± 0.1	1.05 ± 0.1	4.06 ± 0.4	4.09 ± 0.4
1	$0.51 \pm 0.03\,[\frac{1}{2}]$	$0.51 \pm 0.03\,[\frac{1}{2}]$	$2.00 \pm 0.1\,[2]$	$1.99 \pm 0.1\,[2]$
2	1.03 ± 0.1	1.02 ± 0.1	4.02 ± 0.4	4.00 ± 0.4
3	0.51 ± 0.05	0.51 ± 0.05	4.00 ± 0.4	3.99 ± 0.4
4	1.0 ± 0.15	1.01 ± 0.15	6.05 ± 0.9	6.00 ± 0.9
5	0.51 ± 0.15	0.52 ± 0.16	6.20 ± 1.9	5.82 ± 1.7

Table A.1: Postbuckling profile scaling exponents of Δu and t, for the expansion of the nominal strain and stress profiles as defined in Eqs. (A.1a-A.2b). Each row corresponds to a different order of n and values within the square brackets represent analytical results as predicted by Euler's elastica for clamped-clamped boundary conditions.

and

$$\frac{\sigma - \sigma_b}{E}\left(t, \Delta u, \frac{x}{w}\right) = \sum_{n=0} D_n\left(t, \Delta u\right)\left(\frac{x}{w}\right)^n, \tag{A.1b}$$

where C_n and D_n are the coefficients of the expansion in x/w of order n. We refer to these coefficients as the *postbuckling profile coefficients.* At buckling ($\Delta u = 0$), $C_n = D_n = 0$, so it is natural to assume that the postbuckling profile coefficients C_n and D_n grow as power laws in t and Δu in the postbuckling regime. Therefore, we postulate:

$$C_n\left(t, \Delta u\right) = \bar{C}_n t^{\alpha_n} \Delta u^{\beta_n}, \tag{A.2a}$$

and

$$D_n\left(t, \Delta u\right) = \bar{D}_n t^{\rho_n} \Delta u^{\tau_n}. \tag{A.2b}$$

Here, α_n, β_n, ρ_n and τ_n are *postbuckling profile scaling exponents* and $\bar{C}_n$ and $\bar{D}_n$ are the *postbuckling profile prefactors* which we will now determine up to the order $n = 5$ from our numerical simulations.

To determine all the constants, we use the numerical protocol described in Section 2.1.3 and perform $N = 10^2$ simulations for beams with a logarithmically spaced width-to-length ratio in the range from $t = 0.01$ up to $t = 0.25$, and with an excess strain that is increased from $\Delta u = 10^{-3}$ up to $\Delta u = 1$ in 3×10^2 subsequent steps. For each simulation we extract the spatial shape of the nominal stress and strain as function of x/w across the middle of the beam at $s = \ell/2$ and fit $\varepsilon(x)$ and $\sigma(x)/E$ to polynomials of order $n = 5$, by which we obtain the postbuckling profile coefficients $C_n(t, \Delta u)$ and $D_n(t, \Delta u)$ for each specific set of parameter values t and Δu. From these quantities we subsequently deduce the postbuckling profile scaling exponents and prefactors up to order $n = 5$.

n	$\bar{C}_n$	$\bar{D}_n$	$\bar{C}_n/\bar{D}_n$
0	72.0 ± 25	38.3 ± 13	1.88 ± 0.9
1	$21.3 \pm 3.2 \left[\frac{4\pi^2}{\sqrt{3}} \approx 22.8\right]$	$21.1 \pm 3.2 \left[\frac{4\pi^2}{\sqrt{3}} \approx 22.8\right]$	1.01 ± 0.2 [1]
2	-116 ± 41	-553 ± 194	0.21 ± 0.1
3	320 ± 112	254.9 ± 89	1.26 ± 0.6
4	$-6.1 \cdot 10^3 \pm 2.4 \cdot 10^3$	$-1.4 \cdot 10^4 \pm 5.6 \cdot 10^3$	0.42 ± 0.2
5	$1.1 \cdot 10^4 \pm 5.5 \cdot 10^3$	$1.2 \cdot 10^4 \pm 6 \cdot 10^3$	0.99 ± 0.7

Table A.2: Postbuckling profile prefactors $\bar{C}_n$ and $\bar{D}_n$ and their ratio, for the expansion of the nominal strain and stress profiles as defined in Eq. (A.1a-A.2b). Each row corresponds to a different order of n and values within the square brackets represent analytical results, predicted by Euler's elastica for clamped-clamped boundary conditions.

The results of this fitting procedure, shown in Fig. A.6 and Tables (A.1-A.2)) confirm the validity of the polynomial asymptotic decomposition Eqs. (A.1a-A.2b). In the following, we carry out a similar analysis for shear deformations.

Appendix A.2. Series expansion of the nominal shear stress and strain

Second, we investigate shear effects using a similar expansion as above in the beam transverse coordinate x/w, the beam width-to-length ratio t and the excess displacement $\Delta u \equiv (u - u_c)/u_c$, and determine all prefactors and scaling exponents using our FEM results. Standard beam theories such as Mindlin-Reissner theory assume that the nominal shear stress and strain profiles are constant across the beam. In wide 2D neo-Hookean beams, the deformation field is more complex and we analyze deviations from a constant profile by expanding the nominal shear strain and stress around the buckling strain and stress. Following a similar series expansion as in Eqs. (A.1a-A.2b), we expand the nominal shear strain and stress profiles as:

$$\gamma\left(t, \Delta u, \frac{x}{w}\right) = \sum_{n=0} J_n\left(t, \Delta u\right)\left(\frac{x}{w}\right)^n, \tag{A.3a}$$

and

$$\frac{\tau}{G}\left(t, \Delta u, \frac{x}{w}\right) = \sum_{n=0} K_n\left(t, \Delta u\right)\left(\frac{x}{w}\right)^n, \tag{A.3b}$$

where J_n and K_n are the postbuckling profile coefficients of the expansion at order n. Note that prior to buckling, the beam simply undergoes uniform uniaxial compression and has not developed any curvature yet. Therefore, unlike the uniaxial nominal strain and stress which are constant across the beam in

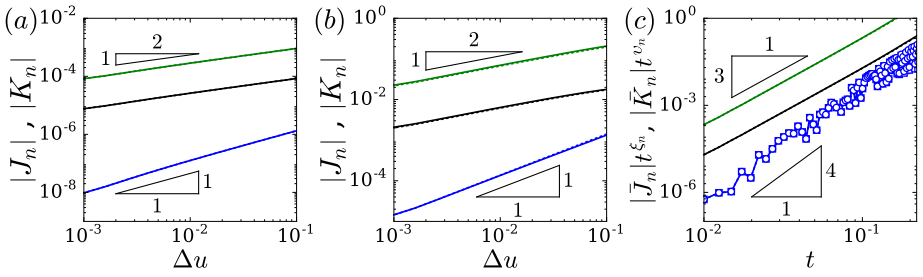

Figure A.7: Dependence of the spatial nominal shear strain and stress profiles on Δu and t, obtained by FEM simulations. In black, blue and green we have plotted the postbuckling profile coefficients J_n (solid lines) and K_n (dashed lines), corresponding to order $n = 0$, $n = 1$ and $n = 2$ respectively. (a-b). We have plotted $|J_n|$ and $|K_n|$ as function of Δu for (a) a slender beam ($t = 0.02$) and (b) a thick beam ($t = 0.15$). (c). Dependence of J_n and K_n on the beam's aspect ratio t.

the prebuckling regime, the shear stress and strain are strictly zero for $\Delta u \leq 0$. Similarly to the postbuckling profile coefficients C_n and D_n (Eqs. (A.2a-A.2b)), we use that $J_n = K_n = 0$ at buckling, and we assume that the postbuckling profile coefficients J_n and K_n grow as power laws in t and Δu in the postbuckling regime:

$$J_n\left(t, \Delta u\right) = \bar{J}_n t^{\xi_n} \Delta u^{\Xi_n}, \tag{A.4a}$$

and

$$K_n\left(t, \Delta u\right) = \bar{K}_n t^{\upsilon_n} \Delta u^{\Upsilon_n}. \tag{A.4b}$$

Here, ξ_n, Ξ_n, υ_n and Υ_n are the postbuckling profile scaling exponents, and $\bar{J}_n$ and $\bar{K}_n$ are the postbuckling profile prefactors which we determine from numerical simulations.

	Δu		t	
n	Ξ_n	Υ_n	ξ_n	υ_n
0	0.49 $\pm$ 0.02	0.49 $\pm$ 0.02	3.02 $\pm$ 0.15	3.01 $\pm$ 0.15
1	1.03 $\pm$ 0.05	1.06 $\pm$ 0.05	3.98 $\pm$ 0.20	3.98 $\pm$ 0.20
2	0.50 $\pm$ 0.03	0.50 $\pm$ 0.03	3.02 $\pm$ 0.15	3.01 $\pm$ 0.15
3	1.02 $\pm$ 0.26	0.93 $\pm$ 0.23	5.93 $\pm$ 1.48	5.70 $\pm$ 1.43

Table A.3: Postbuckling profile scaling exponents of Δu and t, for the expansion of the nominal shear strain and stress profiles as defined in Eq. (A.3a-A.4b). Each row corresponds to a different order of n and results are provided up to cubic order ($n = 3$).

n	$\bar{J}_n$	$\bar{K}_n$	$\bar{J}_n/\bar{K}_n$
0	-18.9 ± 1.9	-18.8 ± 1.9	1.0 ± 0.14
1	-45.3 ± 4.5	-45.3 ± 4.5	1.0 ± 0.14
2	205.9 ± 20.6	204.3 ± 20.4	1.0 ± 0.14
3	$-4.4 \cdot 10^3 \pm 1.8 \cdot 10^3$	$-3.7 \cdot 10^3 \pm 1.5 \cdot 10^3$	1.2 ± 0.68

Table A.4: Postbuckling profile prefactors $\bar{J}_n$ and $\bar{K}_n$ and their ratio, for the expansion of the nominal shear strain and stress profiles as defined in Eqs. (A.3a-A.4b). Each row corresponds to a different order of n and results are provided up to cubic order ($n = 3$).

To determine all the constants, we use the same set of $N = 10^2$ FEM simulations as before, from which we now extract the spatial shape of the nominal shear stress and strain as function of x/w along a cross section at one quarter of the beam, $s = \ell/4$, and fit $\gamma(x)$ and $\tau(x)/G$ to polynomials of order $n = 3$. From the resulting fits we then obtain the postbuckling profile coefficients J_n and K_n for a specific set of parameter values t and Δu. From these quantities we subsequently deduce the postbuckling profile scaling exponents and prefactors up to order $n = 3$. The results of this fitting procedure, shown in Fig. A.6 and Tables (A.1-A.2)) confirm the validity of the polynomial asymptotic decomposition Eqs. (A.1a-A.2b). In the following, we discuss the implications of such asymptotic analysis for the formulation of 1D models.

Appendix A.3. Effective stress-strain relations

In this appendix we set up the appropriate stress-strain relations for both the uniaxial and shear stress-strain relation.

Appendix A.3.1. Nonlinear Uniaxial stress-strain relation

From Table A.2 we see that the coefficients $\bar{C}_n$ and $\bar{D}_n$ are not equal, thus evidencing a nonlinearity in the stress-strain relation. Because the postbuckling slope (Eq. 2) is defined in the vicinity of the buckling point, the starting point is to write a Taylor series for the normal stress around the buckling strain ε_b up to quadratic order, which yields

$$\frac{\sigma - \sigma_b}{E_b} = (\varepsilon - \varepsilon_b) + \eta\,(\varepsilon - \varepsilon_b)^2 + \mathcal{O}\,(\varepsilon - \varepsilon_b)^3\,. \tag{A.5}$$

We can calculate E_b and η analytically by evaluating the expansion in Eq. (A.5) using the stress-strain relation for uniaxially compressed neo-Hookean materials (Ogden, 1997). This yields:

$$E_b\,(\varepsilon_b) = \frac{E}{3}\left(1 + \frac{2}{(1+\varepsilon_b)^3}\right), \tag{A.6a}$$

and

$$\eta\left(\varepsilon_b\right) = -\frac{3}{2\left(1+\varepsilon_b\right)+\left(1+\varepsilon_b\right)^4}. \tag{A.6b}$$

Eq. (A.6a) and Eq. (A.6b) show that as ε_b becomes increasingly negative, both the effective stiffness E_b and the magnitude of nonlinearity parameter η increase. In particular, we find, by expanding Eqs. (A.6a-A.6b) for small ε_b, that the leading order corrections to E_b and η are linear in ε_b:

$$E_b/E = 1 - 2\varepsilon_b + \mathcal{O}\left(\varepsilon_b^2\right), \tag{A.6c}$$

$$\eta = -1 + 2\varepsilon_b + \mathcal{O}\left(\varepsilon_b^2\right). \tag{A.6d}$$

Furthermore, note that as $\varepsilon_b \to 0$, we retrieve $E_b/E = 1$ and $\eta = -1$, in agreement with the small strain limit of uniaxally compressed neo-Hookean materials (Ogden, 1997). Finally, Eq. (A.6d) is also consistent with the value that we can calculate from the numerical constants C_n and D_n using Table A.2, namely:

$$\eta = \frac{D_2 - C_2}{C_1^2} \approx 1 \tag{A.7}$$

Appendix A.3.2. Linear shear stress-strain relation

In addition, we have seen from Table A.4 that the coefficients $\bar{J}_n$ and $\bar{K}_n$ are equal, therefore the nominal shear strain and stress are linearly related, hence we can assume

$$\tau(x) = G\gamma(x), \tag{A.8}$$

which is the result as predicted by Ogden (1997) in the case of simple shear for neo-Hookean materials. We will use this linear constitutive equation for the shear in the remainder of this paper.

Appendix B. Construction of the 1D energy density comprising stress-strain nonlinearity

In this appendix, we construct the energy density based on Mindlin-Reissner kinematics and a nonlinear stress-strain relation and take into account distortions to the Mindlin-Reissner kinematics. This 1D energy density is the base of our models, presented in Section 3 of the main text.

We start by expressing the total increase of the elastic energy beyond buckling. This increase follows from an integral of the respective products of stress

and strain, integrated over the surface area of the beam, that is,

$$\mathcal{E}/d = \int ds\, dx \left(\int_0^{\varepsilon_{xx}} d\varepsilon'_{xx}\sigma_{xx} + \int_0^{\varepsilon_{yy}} d\varepsilon'_{yy}\sigma_{yy} + \int_{\varepsilon_b}^{\varepsilon_{zz}} d\varepsilon'_{zz}\sigma_{zz} + \int_0^{\varepsilon_{xy}} d\varepsilon'_{xy}\sigma_{xy} + \int_0^{\varepsilon_{yz}} d\varepsilon'_{yz}\sigma_{yz} + \int_0^{\varepsilon_{xz}} d\varepsilon'_{xz}\sigma_{xz} \right). \tag{B.1}$$

Even though we consider 2D beams, we keep a factor d (the depth) here to facilitate comparison to 3D beam results. For 2D beams, the 'yy', 'xy' and 'yz' contributions are zero. Moreover, since the beam can freely expand along the x direction without any barrelling effects near the boundaries, we expect that $\sigma_{xx} \approx 0$ at each point of the beam, an assumption which we have verified numerically in our 2D simulations. As a result, we are left with the 'zz' and 'xz' terms, which correspond to the uniaxial and shear deformations, respectively. Our aim is to set up an energy functional using the Mindlin-Reissner strains — 1D fields describing the shape of the beam along the curvilinear coordinate s.

Therefore we define a linear energy density $\epsilon(s)$ as follows:

$$\mathcal{E} = \int_0^{\ell} ds\, \epsilon(s), \tag{B.2a}$$

where

$$\frac{\epsilon(s)}{d} = \int_{-\frac{w}{2}}^{\frac{w}{2}} dx \int_{\varepsilon_b}^{\varepsilon(x)} \sigma\left(\varepsilon'\right) d\varepsilon' + \int_{-\frac{w}{2}}^{\frac{w}{2}} dx \int_{\varepsilon_b}^{\gamma(x)} \tau\left(\gamma'\right) d\gamma', \tag{B.2b}$$

with $\varepsilon \equiv \varepsilon_{zz}$ and $\gamma \equiv \varepsilon_{xz}$. Here, $\epsilon(s)$ represents the linear energy density that captures the amount of energy in a cross sectional area of the beam per unit length of the curvilinear coordinate s.

Appendix B.1. 1D energy density including distortions from Mindlin-Reissner kinematics

Here we present the energy density comprising distortions from the Mindlin-Reissner strains and built with the aid of the numerical results. To this end, we substitute the respective stress-strain relations (Eq. (A.5) and Eq. (A.8)) to carry out the integration with respect to the nominal strains ε and γ. Second, we integrate with respect to x by using the expansions of the uniaxial and shear strain profiles up to cubic order (Eqs. (A.1a) and (A.3a)). This yields:

$$\begin{aligned}
\frac{\epsilon}{E_b A} = & \left\{ \frac{\bar{C}_1^2}{24} \right\} \Delta u\, t^4 \\
& + \left\{ \frac{\bar{C}_1 \bar{C}_3}{80} + \bar{C}_0 \bar{C}_B + \frac{\bar{C}_2 \bar{C}_B}{12} + \frac{G}{E_b} \left(\frac{1}{2} \bar{J}_0^2 + \frac{1}{12} \bar{J}_0 \bar{J}_2 + \frac{1}{160} \bar{J}_2^2 \right) \right\} \Delta u\, t^6 \\
& + \left\{ \frac{\bar{C}_3^2}{896} + \left(\frac{\bar{C}_0^2}{2} + \frac{\bar{C}_0 \bar{C}_2}{12} + \frac{\bar{C}_2^2}{160} + \eta \frac{\bar{C}_0 \bar{C}_1^2}{12} + \eta \frac{\bar{C}_1^2 \bar{C}_2}{80} + \frac{G}{24 E_b} \bar{J}_1^2 \right) \Delta u \right\} \Delta u\, t^8 \\
& + \mathcal{O}\left(\Delta u^2 t^{10} \right).
\end{aligned}$$

(B.3)

We have now established carefully the beam's energy density up to second order in excess strain and eighth order width-to-length ratio, $\mathcal{O}\left(\Delta u^2 t^8\right)$. The above analysis identifies and quantifies precisely how nonlinearity in stress-strain laws and distortions to Mindlin-Reissner kinematics alter the 1D energy density formulation. While the order $\mathcal{O}(\Delta u\, t^4)$ corresponds exactly to Euler's elastica, the order $\mathcal{O}(\Delta u\, t^6)$ comprises the classical Timenshenko beam contribution as well as distortions from the linear bending profile. The order $\mathcal{O}(\Delta u\, t^8)$ contains the nonlinearity η as well as further distortions for bending and shear.

After a few manipulations which we explain hereafter, it can be shown that Eq. (B.3) can be converted in terms of the Mindlin-Reissner strains as:

$$\begin{aligned}\frac{\epsilon}{E_b} = A\varepsilon_b\,\varepsilon_0 + \frac{1}{2}A\zeta_2(\eta)\varepsilon_0^2 + I\left(\frac{1}{2}\zeta_1(t) + \eta\,\varepsilon_0\right)\varepsilon_1^2 \\ + \frac{GA}{2E_b}\,\gamma_0^2\left(k_1 + k_2\gamma_0^2\right),\end{aligned} \tag{B.4a}$$

where the coefficients $\zeta_1(t)$ and $\zeta_2(\eta)$ are given by

$$\zeta_1(t) = 1 + 2\left(\frac{\bar{C}_2\bar{C}_B}{\bar{C}_1^2} + \frac{3}{20}\frac{\bar{C}_3}{\bar{C}_1}\right)t^2 + \frac{3}{112}\left(\frac{\bar{C}_3}{\bar{C}_1}\right)^2 t^4, \tag{B.4b}$$

$$\zeta_2(\eta) = 1 + \frac{1}{6}\frac{\bar{C}_2}{\bar{C}_0}\left(1 + \frac{3}{40}\frac{\bar{C}_2}{\bar{C}_0} + \frac{3}{20}\eta\frac{\bar{C}_1^2}{\bar{C}_0}\right), \tag{B.4c}$$

and where k_1 and k_2 are given by

$$k_1 = 1 + \frac{1}{6}\frac{\bar{J}_2}{\bar{J}_0} + \frac{1}{80}\left(\frac{\bar{J}_2}{\bar{J}_0}\right)^2, \tag{B.4d}$$

and

$$k_2(t) = \frac{1}{12}\frac{\bar{J}_1^2}{\bar{J}_0^4}t^{-4}. \tag{B.4e}$$

To obtain the above results we have used the fact that there is a clear pattern in the scaling exponents of the higher order corrections of the uniaxial and shear strain profiles with the excess displacement Δu, which alternate between $1/2$ or 1 (see Tables A.1 and A.3). Consequently, we can factorize the Δu dependence and express the higher order corrections in terms of the Mindlin-Reissner strains. For example, the quadratic postbuckling profile coefficient of the axial strain profile, $C_2 = \bar{C}_2\Delta u\, t^4$, can be expressed in terms of $\varepsilon_0 \equiv C_0 = \bar{C}_0\Delta u\, t^4$ as $C_2 = \left(\bar{C}_2/\bar{C}_0\right)\varepsilon_0$.

Antman, S. S., 1972. The theory of rods. In: Handbuch der Physik. Vol. VIa/2. Springer, pp. 641–703.

Antman, S. S., Pierce, J. F., 1990. The intricate global structure of buckled states of compressible columns. SIAM Journal on Applied Mathematics 50 (2), 395–419.

Antman, S. S., Rosenfeld, G., 1978. Global behavior of buckled states of nonlinearly elastic rods. Siam Review 20 (3), 513–566.

Ashby, M., Brechet, Y., 2003. Designing hybrid materials. Acta materialia 51 (19), 5801–5821.

Audoly, B., Jul 2011. Localized buckling of a floating elastica. Phys. Rev. E 84, 011605.
URL http://link.aps.org/doi/10.1103/PhysRevE.84.011605

Autumn, K., Liang, Y. A., Hsieh, S. T., Zesch, W., Chan, W. P., Kenny, T. W., Fearing, R., Full, R. J., 2000. Adhesive force of a single gecko foot-hair. Nature 405 (6787), 681–685.

Bažant, Z. P., Cedolin, L., 2010. Stability of structures: elastic, inelastic, fracture and damage theories. World Scientific.

Biggins, J. S., Saintyves, B., Wei, Z., Bouchaud, E., Mahadevan, L., 2013. Digital instability of a confined elastic meniscus. Proceedings of the National Academy of Sciences 110 (31), 12545–12548.
URL http://www.pnas.org/content/110/31/12545.abstract

Boyce, M. C., Arruda, E. M., 2000. Constitutive models of rubber elasticity: A review. Rubber Chemistry and Technology 73 (3), 504–523.
URL http://dx.doi.org/10.5254/1.3547602

Brenner, M. P., Lang, J. H., Li, J., Qiu, J., Slocum, A. H., 2003. Optimal design of a bistable switch. PNAS (Proceedings of the National Academy of Sciences) 100 (17), 9663–9667.
URL http://www.pnas.org/content/100/17/9663.abstract

Budiansky, B., 1974. Theory of buckling and post-buckling behavior of elastic structures. Advances in Applied Mechanics 14, 1–65.

Cao, Y., Hutchinson, J. W., 2011. From wrinkles to creases in elastomers: the instability and imperfection-sensitivity of wrinkling. Proceedings of the Royal Society of London A: Mathematical, Physical and Engineering Sciences 468 (2137), 94–115.
URL http://rspa.royalsocietypublishing.org/content/468/2137/94

Castañeda, P., 1991. The effective mechanical properties of nonlinear isotropic composites. Journal of the Mechanics and Physics of Solids 39 (1), 45 – 71.
URL http://www.sciencedirect.com/science/article/pii/002250969190030R

Cho, Y., Shin, J.-H., Costa, A., Kim, T. A., Kunin, V., Li, J., Lee, S. Y., Yang, S., Han, H. N., Choi, I.-S., Srolovitz, D. J., 2014. Engineering the shape and structure of materials by fractal cut. Proceedings of the National Academy of Sciences 111 (49), 17390–17395.
URL http://www.pnas.org/content/111/49/17390.abstract

Coulais, C., 2016. Periodic cellular materials with nonlinear elastic homogenized stress-strain response at small strains. International Journal of Solids and Structures 97–98, 226–238.
URL http://www.sciencedirect.com/science/article/pii/S002076831630186X

Coulais, C., Overvelde, J. T. B., Lubbers, L. A., Bertoldi, K., van Hecke, M., Jul 2015. Discontinuous buckling of wide beams and metabeams. Phys. Rev. Lett. 115, 044301.
URL http://link.aps.org/doi/10.1103/PhysRevLett.115.044301

Coulais, C., Sounas, D., Alù, A., 02 2017. Static non-reciprocity in mechanical metamaterials. Nature 542 (7642), 461–464.

Coulais, C., Teomy, E., de Reus, K., Shokef, Y., van Hecke, M., 07 2016. Combinatorial design of textured mechanical metamaterials. Nature 535 (7613), 529–532.
URL http://dx.doi.org/10.1038/nature18960

Cowper, G. R., Jun 1966. The shear coefficient in timoshenko's beam theory. J. Appl. Mech. 33 (2), 335–340.
URL http://dx.doi.org/10.1115/1.3625046

Danas, K., Triantafyllidis, N., 2014. Instability of a magnetoelastic layer resting on a non-magnetic substrate. Journal of the Mechanics and Physics of Solids 69, 67–83.

Davies, J., Leach, P., Heinz, D., 1994. Second-order generalised beam theory. Journal of Constructional Steel Research 31 (2), 221–241.

Diamant, H., Witten, T. A., Oct 2011. Compression induced folding of a sheet: An integrable system. Phys. Rev. Lett. 107, 164302.
URL http://link.aps.org/doi/10.1103/PhysRevLett.107.164302

Doghri, I., 2013. Mechanics of deformable solids: linear, nonlinear, analytical and computational aspects. Springer Science & Business Media.

Euler, L., 1774. Additamentum i de curvis elasticis, methodus inveniendi lineas curvas maximi minimivi proprietate gaundentes. Opera Omnia I 24 (1744), 232–297.

Florijn, B., Coulais, C., van Hecke, M., Oct 2014. Programmable mechanical metamaterials. Phys. Rev. Lett. 113, 175503.
URL http://link.aps.org/doi/10.1103/PhysRevLett.113.175503

Frenzel, T., Findeisen, C., Kadic, M., Gumbsch, P., Wegener, M., 2016. Tailored buckling microlattices as reusable light-weight shock absorbers. Adv. Mater. URL http://www.ncbi.nlm.nih.gov/pubmed/27159205

Geymonat, G., Müller, S., Triantafyllidis, N., 1993. Homogenization of nonlinearly elastic materials, microscopic bifurcation and macroscopic loss of rank-one convexity. Archive for Rational Mechanics and Analysis 122 (3), 231–290. URL http://dx.doi.org/10.1007/BF00380256

Gibson, L. J., Ashby, M. F., 1997. Cellular Solids: Structure and Properties (Cambridge Solid State Science Series). Cambridge University Press.

Gladman, A. S., Matsumoto, E. A., Nuzzo, R. G., Mahadevan, L., Lewis, J. A., 2016. Biomimetic 4d printing. Nature materials.

Goriely, A., Vandiver, R., Destrade, M., 2008. Nonlinear Euler buckling. Proceedings of the Royal Society of London A: Mathematical, Physical and Engineering Sciences 464 (2099), 3003–3019. URL http://rspa.royalsocietypublishing.org/content/464/2099/3003

Goto, Y., Tomoo, Y., Makoto, O., 1990. Elliptic integral solutions of plane elastica with axial and shear deformations. International journal of solids and structures 26 (4), 375–390.

Goto, Y., Yamashita, T., Matsuura, S., 1987. Elliptic integral solutions for extensional elastica with constant initial curvature. Struct. Engng./Earthquake Engng 4 (2), 299–309.

Guckenheimer, J., Holmes, P., 1983. Nonlinear oscillations, dynamical systems, and bifurcations of vector fields. Vol. 42. Springer Science & Business Media.

Holmes, D., Crosby, A., 2007. Snapping surfaces. Advanced Materials 19 (21), 3589–3593. URL http://dx.doi.org/10.1002/adma.200700584

Holmes, D. P., Roche, M., Sinha, T., Stone, H. A., 2011. Bending and twisting of soft materials by non-homogenous swelling. Soft Matter 7, 5188–5193. URL http://dx.doi.org/10.1039/C0SM01492C

Huang, J., Juszkiewicz, M., de Jeu, W. H., Cerda, E., Emrick, T., Menon, N., Russell, T. P., 2007. Capillary wrinkling of floating thin polymer films. Science 317 (5838), 650–653. URL http://science.sciencemag.org/content/317/5838/650

Humer, A., 2013. Exact solutions for the buckling and postbuckling of shear-deformable beams. Acta Mechanica 224 (7), 1493–1525. URL http://dx.doi.org/10.1007/s00707-013-0818-1

Hutchinson, J., Koiter, W., 1970. Postbuckling theory. Appl. Mech. Rev 23 (12), 1353–1366.

Hutchinson, J. R., Aug 2000. Shear coefficients for timoshenko beam theory. J. Appl. Mech. 68 (1), 87–92.
URL http://dx.doi.org/10.1115/1.1349417

Irschik, H., Gerstmayr, J., 2009. A continuum mechanics based derivation of reissner's large-displacement finite-strain beam theory: the case of plane deformations of originally straight bernoulli–euler beams. Acta Mechanica 206 (1), 1–21.

Kim, J., Hanna, J. A., Byun, M., Santangelo, C. D., Hayward, R. C., 2012. Designing responsive buckled surfaces by halftone gel lithography. Science 335 (6073), 1201–1205.
URL http://science.sciencemag.org/content/335/6073/1201

Li, T., Keplinger, C., Baumgartner, R., Bauer, S., Yang, W., Suo, Z., 2013. Giant voltage-induced deformation in dielectric elastomers near the verge of snap-through instability. Journal of the Mechanics and Physics of Solids 61 (2), 611–628.

Lopez-Pamies, O., Castañeda, P. P., 2006a. On the overall behavior, microstructure evolution, and macroscopic stability in reinforced rubbers at large deformations: II—Application to cylindrical fibers. Journal of the Mechanics and Physics of Solids 54 (4), 831 – 863.
URL http://www.sciencedirect.com/science/article/pii/S0022509605002036

Lopez-Pamies, O., Castañeda, P. P., 2006b. On the overall behavior, microstructure evolution, and macroscopic stability in reinforced rubbers at large deformations: I—theory. Journal of the Mechanics and Physics of Solids 54 (4), 807 – 830.
URL http://www.sciencedirect.com/science/article/pii/S0022509605002024

Magnusson, A., Ristinmaa, M., Ljung, C., 2001. Behaviour of the extensible elastica solution. Int. J. Sol. Struct. 38 (46–47), 8441 – 8457.
URL http://www.sciencedirect.com/science/article/pii/S0020768301000890

Marion, J. B., 2013. Classical dynamics of particles and systems. Academic Press.

Mazzilli, C. E., 2009. Buckling and post-buckling of extensible rods revisited: A multiple-scale solution. International Journal of Non-Linear Mechanics 44 (2), 200–208.

Michel, J.-C., Lopez-Pamies, O., Castañeda, P. P., Triantafyllidis, N., 2007. Microscopic and macroscopic instabilities in finitely strained porous elastomers. Journal of the Mechanics and Physics of Solids 55 (5), 900–938.

Moon, M.-W., Lee, S. H., Sun, J.-Y., Oh, K. H., Vaziri, A., Hutchinson, J. W., 2007. Wrinkled hard skins on polymers created by focused ion beam. Proceedings of the National Academy of Sciences 104 (4), 1130–1133.
URL http://www.pnas.org/content/104/4/1130.abstract

Mullin, T., Deschanel, S., Bertoldi, K., Boyce, M. C., Aug 2007. Pattern transformation triggered by deformation. Phys. Rev. Lett. 99, 084301.
URL http://link.aps.org/doi/10.1103/PhysRevLett.99.084301

Na, J.-H., Bende, N. P., Bae, J., Santangelo, C. D., Hayward, R. C., 2016. Grayscale gel lithography for programmed buckling of non-euclidean hydrogel plates. Soft Matter, –.
URL http://dx.doi.org/10.1039/C6SM00714G

Narayanasamy, R., Murthy, R., Viswanatham, K., Chary, G., 1988. Prediction of the barreling of solid cylinders under uniaxial compressive load. Journal of mechanical working technology 16 (1), 21–30.

Nasto, A., Ajdari, A., Lazarus, A., Vaziri, A., Reis, P. M., 2013. Localization of deformation in thin shells under indentation. Soft Matter 9 (29), 6796–6803.

Ogden, R. W., 1997. Non Linear Elasic Deformations. Dover Publ.

Overvelde, J. T. B., Kloek, T., D'haen, J. J. A., Bertoldi, K., 2015. Amplifying the response of soft actuators by harnessing snap-through instabilities. Proceedings of the National Academy of Sciences 112 (35), 10863–10868.
URL http://www.pnas.org/content/112/35/10863.abstract

Pezzulla, M., Shillig, S. A., Nardinocchi, P., Holmes, D. P., 2015. Morphing of geometric composites via residual swelling. Soft Matter 11, 5812–5820.
URL http://dx.doi.org/10.1039/C5SM00863H

Pflüger, A., 2013. Stabilitätsprobleme der Elastostatik. Springer-Verlag.

Pocivavsek, L., Dellsy, R., Kern, A., Johnson, S., Lin, B., Lee, K. Y. C., Cerda, E., 2008. Stress and fold localization in thin elastic membranes. Science 320 (5878), 912–916.
URL http://science.sciencemag.org/content/320/5878/912

Raney, J. R., Nadkarni, N., Daraio, C., Kochmann, D. M., Lewis, J. A., Bertoldi, K., 2016. Stable propagation of mechanical signals in soft media using stored elastic energy. Proc Natl Acad Sci U S A 113 (35), 9722–7.
URL https://www.ncbi.nlm.nih.gov/pubmed/27519797

Reis, P. M., 2015. A perspective on the revival of structural (in) stability with novel opportunities for function: From buckliphobia to buckliphilia. Journal of Applied Mechanics 82 (11), 111001.

Reis, P. M., Jaeger, H. M., van Hecke, M., 2015. Designer matter: A perspective. Extreme Mechanics Letters 5, 25 – 29.
URL http://www.sciencedirect.com/science/article/pii/S2352431615300080

Reiss, E. L., 1969. Column buckling—an elementary example of bifurcation. Bifurcation theory and nonlinear eigenvalue problems, 1–16.

Reissner, E., 1972. On one-dimensional finite-strain beam theory: The plane problem. Zeitschrift für angewandte Mathematik und Physik ZAMP 23 (5), 795–804.
URL http://dx.doi.org/10.1007/BF01602645

Reissner, E., 1973. On one-dimensional large-displacement finite-strain beam theory. Studies in applied mathematics 52 (2), 87–95.

Sharma, A., Licup, A. J., Jansen, K. A., Rens, R., Sheinman, M., Koenderink, G. H., MacKintosh, F. C., 01 2016. Strain-controlled criticality governs the nonlinear mechanics of fibre networks. Nat Phys advance online publication, –.
URL http://dx.doi.org/10.1038/nphys3628

Shepherd, R. F., Ilievski, F., Choi, W., Morin, S. A., Stokes, A. A., Mazzeo, A. D., Chen, X., Wang, M., Whitesides, G. M., 2011. Multigait soft robot. PNAS (Proceedings of the National Academy of Sciences) 108 (51), 20400–20403.
URL http://www.pnas.org/content/108/51/20400.abstract

Shim, J., Perdigou, C., Chen, E. R., Bertoldi, K., Reis, P. M., 2012. Buckling-induced encapsulation of structured elastic shells under pressure. Proceedings of the National Academy of Sciences 109 (16), 5978–5983.
URL http://www.pnas.org/content/109/16/5978.abstract

Simo, J. C., 1985. A finite strain beam formulation. the three-dimensional dynamic problem. part i. Computer methods in applied mechanics and engineering 49 (1), 55–70.

Simo, J. C., Vu-Quoc, L., 1986. A three-dimensional finite-strain rod model. part ii: Computational aspects. Computer methods in applied mechanics and engineering 58 (1), 79–116.

Simo, J. C., Vu-Quoc, L., 1988. On the dynamics in space of rods undergoing large motions—A geometrically exact approach. Computer methods in applied mechanics and engineering 66 (2), 125–161.

Simo, J. C., Vu-Quoc, L., 1991. A geometrically-exact rod model incorporating shear and torsion-warping deformation. International Journal of Solids and Structures 27 (3), 371–393.

Terwagne, D., Brojan, M., Reis, P. M., 2014. Smart surfaces: Smart morphable surfaces for aerodynamic drag control (adv. mater. 38/2014). Advanced Materials 26 (38), 6659–6659.
URL http://dx.doi.org/10.1002/adma.201470262

Timoshenko, S., MAY 1921. On the correction for shear of the differential equation for transverse vibrations of prismatic bars. Philos. Mag. 41 (245, 6TH SERIES), 744–746.

Timoshenko, S., Goodier, J., 1970. Theory of Elasticity. 3rd edition.

Timoshenko, S. P., Gere, J. M., 1961. Theory of elastic stability. 1961. McGrawHill-Kogakusha Ltd, Tokyo, 109.

Vaz, M., Silva, D., 2003. Post-buckling analysis of slender elastic rods subjected to terminal forces. International journal of non-linear mechanics 38 (4), 483–492.

Wang, C., 1997. Post-buckling of a clamped-simply supported elastica. International Journal of Non-Linear Mechanics 32 (6), 1115–1122.

Wang, P., Casadei, F., Shan, S., Weaver, J. C., Bertoldi, K., 2014. Harnessing buckling to design tunable locally resonant acoustic metamaterials. Physical review letters 113 (1), 014301.

Wang, Q., Suo, Z., Zhao, X., 2012. Bursting drops in solid dielectrics caused by high voltages. Nature communications 3, 1157.

Yang, S., Choi, I.-S., Kamien, R. D., 2 2016. Design of super-conformable, foldable materials via fractal cuts and lattice kirigami. MRS Bulletin 41, 130–138.
URL http://journals.cambridge.org/article_S0883769416000051

Yoon, J., Cai, S., Suo, Z., Hayward, R. C., 2010. Poroelastic swelling kinetics of thin hydrogel layers: comparison of theory and experiment. Soft Matter 6, 6004–6012.
URL http://dx.doi.org/10.1039/C0SM00434K